Higher-order narrow-tube quantizations of quasienergies

1998 J. Phys. A: Math. Gen. 31 2253

(http://iopscience.iop.org/0305-4470/31/9/013)

J. Phys. A: Math. Gen. **31** (1998) 2253–2267. Printed in the UK PII: S0305-4470(98)86936-9

Higher-order narrow-tube quantizations of quasienergies

Karl-Erik Thylwe

Department of Mechanics, Royal Institute of Technology, S-100 44 Stockholm, Sweden

Received 18 August 1997, in final form 31 October 1997

Abstract. The narrow-tube quasienergy quantization allows an identification of part of the spectrum due to stable elliptic islands of the period map. With its transparent connection to the classical dynamics it also sets an absolute scale to the understanding of the Brillouin zone spectrum of quasienergies. In combination with a recent time-dependent normal-form expansion we show that the applicability and accuracy of the narrow-tube quantization is improved. Its analytic form helps us understand the quasiregular motion centred near periodic responses. We numerically consider harmonic and subharmonic elliptic islands of the weakly nonlinear Duffing oscillator.

1. Introduction

There is a current theoretical development of corrections to leading-order semiclassical quantization formulae [1, 2]. The successes of the WKB (Wentzel–Kramers–Brillouin) and phase-integral methods of separable dynamics are well documented [3]. In the same spirit, it is useful to have accurate quantization formulae such as those associated with locally regular motion of mixed systems. In this paper we consider a time-dependent Hamiltonian system with a mixed regular and irregular phase space.

The recent development of a higher-order time-dependent normal form [4] and its asymptotic (adiabatic) expansion [5] is suited for this purpose. This is a further development of the narrow-tube framework presented in [6]. We report the first application of this recent formalism to a time-periodic Hamiltonian Duffing system. In particular we investigate the limitations as to resonance phenomena.

The relation between the narrow-tube quantization and the semiclassical EBK (Einstein–Brillouin–Keller) quantization of time-periodic systems [7, 8] is of importance in this work. The EBK calculations are performed numerically from classical phase-space data (where sometimes interpolations between tori data are required) and, like its Bohr–Sommerfeld counterpart in one dimension, the result can only occasionally coincide with exact quantal results. The main difference is that Bohr–Sommerfeld's formula does not need numerical phase-space data in the calculation. Hence, there are typical errors involved in the EBK results of higher order in $\overline{h}$.

In the higher-order narrow-tube framework the results can in principle be asymptotically correct, depending on the *localization*. This is merely a quantum tail effect of a finite shifting of the boundary conditions, resulting in exponentially small corrections. However, the localization of the wavefunction may not be trivially satisfied (see Howland [9] and Hone *et al* [10]) for all oscillators, and even if it seems to be justified for the confining repulsive Duffing oscillator, the localization means that one neglects effects due to tunnelling communication with the outside of the main elliptic island.

0305-4470/98/092253+15$19.50

Assuming that the localization is justified, the occurrences of elliptic subharmonic chains and the associated stochastic separatrix layers inside the main elliptic island manifest themselves as singularities in the corresponding orders of the present narrow-tube quantization, as in all (non-resonant) normal-form theories. The low-order narrow-tube quantization thus neglects classical irregularities belonging to higher orders, which means a smoothening of the true quasienergy spectrum as a function of some physical system parameter.

If the narrow-tube quantization is sufficiently convergent, there is outlined in [4, 5] a systematic phase-integral expansion of the relevant narrow-tube quantities that correspond to a semiclassical expansion.

A particular objective of the present investigation is to clarify the observation in [6] that the *large-amplitude* elliptic centre of the weakly driven Duffing system was strikingly better described by the first-order narrow-tube quantization than the *small-amplitude* elliptic centre was. In this work we can analyse the contributions of the subsequent order in detail to find an explanation.

Section 2 outlines the time-dependent normal-form procedure unified with the narrow-tube quantization. The limitations of the procedure due to resonances are discussed in section 3. The formulae are applied in section 4 to a periodically excited Duffing oscillator, which has been studied both semiclassically and quantum mechanically. Quasiregular motion centred on T-periodic and $3T$-periodic responses are analysed. Conclusions are given in section 5.

2. Outline of the narrow-tube quantization

In this section we summarize the essential steps in the higher-order narrow-tube quantization procedure, leaving particular details for the specific Hamiltonian Duffing oscillator to section 4.

A time-periodic Hamiltonian oscillator of the form

$$H(p_x, x, t) = \tfrac{1}{2}p_x^2 + V(x, t) \tag{1}$$

with the external T-periodic condition

$$V(x, t + T) = V(x, t) \tag{2}$$

may support a mixture of regular and chaotic dynamics. A family of regular classical trajectories is typically centred around each stable periodic orbit (dynamical equilibrium, elliptic centre) of the system, with a characteristic period T_p rationally related to T. A linear systems would have just a single periodic response 'organizing' a single family of regular dynamics.

The Hamiltonian can be subject to a canonical T_p-periodic centre transformation ($x = x_p(t) + q$, $p_x = \dot{x}_p(t) + p$), as described in [11], where the new 'centre' Hamiltonian takes the form:

$$H(p, q, t) = -L_p(t) + \tfrac{1}{2}p^2 + \tfrac{1}{2}h_2(t)q^2 + \tfrac{1}{3}h_3(t)q^3 + \tfrac{1}{4}h_4(t)q^4 + \cdots \tag{3}$$

$L_p(t)$ being the Lagrangian of the T_p-periodic centre trajectory and the periodic behaviours of $h_j(t)$, $j = 2, 3, \ldots$ are also due to the underlying centre motion. The coefficient function $h_2(t)$ plays a key role and its specific periodicity will be denoted T_F (Floquet-period), since it may be $T_F = T_p/2$ for certain symmetric trajectories, which we shall see later. This is the first step in the local quantization of elliptic islands of the external period-T map.

In a second step we propose the time-dependent normal-form transformation, described in detail by Thylwe and Dancowicz [4], yielding the transformed Hamiltonian

$$\mathcal{K}_{TD}(\mathcal{L}_N, t) = -L_p(t) + \eta_1(t)\mathcal{L}_N + \eta_2(t)\mathcal{L}_N^2 + \eta_3(t)\mathcal{L}_N^3 + \cdots + \eta_N(t)\mathcal{L}_N^N \tag{4}$$

where $\mathcal{L}_N$ is the Ermakov–Lewis invariant corresponding to the truncation order N of the canonical expansion, and the new coefficients are periodic with periods T_p or T_F. The semiclassical narrow-tube quantization, as introduced in [11], corresponds to the linear expansion ($N = 1$) in (4) with $\mathcal{L}_1$. The coefficient $\eta_1(t)$ has the particular relevance of being the angular velocity of the linearized vortex flow in phase space. As we shall see later, it has the same periodicity T_F as the 'linear' coefficient $h_2(t)$.

At the time of the formulation of the narrow-tube quantization [6], the higher-order terms in the time-dependent normal form were not defined. It turns out that the higher-order coefficient functions exist and are periodic provided the centre motion is sufficiently non-resonant. We return to this delicate point later in connection with the analysis of the Duffing oscillator.

In a final step we can quantize the separable time-periodic Hamiltonian (4). For the 'space' variables, we quantize a Cartesian relation [11]

$$\mathcal{L} = (P^2 + Q^2)/2 \tag{5}$$

independent of the index N of the truncation order, obtaining an ordinary differential equation of the time-independent Schrödinger type:

$$\frac{\mathrm{d}^2\Psi}{\mathrm{d}Q^2} + \frac{1}{\hbar^2}(2\mathcal{L} - Q^2)\Psi = 0. \tag{6}$$

The 'spatial' wavefunction $\Psi(Q)$ satisfies the boundary conditions of *localization* around the centre motion:

$$\Psi(Q) \to 0 \qquad \text{as } |Q| \to \infty \tag{7}$$

which leads to

$$\mathcal{L}_n = (n + \tfrac{1}{2})\hbar \qquad n = 0, 1, \ldots. \tag{8}$$

The quantization in time of the Hamiltonian (4) turns into another ordinary differential equation:

$$\mathcal{K}_{TD}(\mathcal{L}_n, t)\Phi = \mathrm{i}\hbar\frac{\mathrm{d}\Phi}{\mathrm{d}t} \tag{9}$$

which is trivially solved. The resulting wavefunction is a product of a spatial part and a temporal one:

$$Y(\mathcal{L}_n; Q, t) = \Psi(\mathcal{L}_n; Q)\exp\left(-\frac{\mathrm{i}}{\hbar}\int_0^t \mathcal{K}_{TD}(\mathcal{L}_n, t')\,\mathrm{d}t'\right). \tag{10}$$

It remains to identify the quasienergy (ϵ) by constructing the permissible Floquet decompositions of the wavefunction, which leads to the expression:

$$\epsilon_{n,m} = \frac{1}{T_p}\int_0^{T_p} \mathcal{K}_{TD}(\mathcal{L}_n, t')\,\mathrm{d}t' + 2\pi m\hbar/T_p \qquad n = 0, 1, \ldots \qquad m = 0, \pm1, \pm2, \ldots. \tag{11}$$

We notice the interesting connection between the quantal quasienergy and the time-average of the proper normal-form Hamiltonian $\mathcal{K}_{TD}$. One can verify for the forced linear oscillator [7], that this average value is different from the long-time trajectory average of the original Hamiltonian, but of course identical to the long-time trajectory average of

$\mathcal{K}_{TD}$. Nevertheless, the *principal quasienergy* $\epsilon_{n,0}$ of an elliptic island has a clear classical interpretation as an average energy in terms of the proper centre Hamiltonian. The only nontrivial calculations involved are related to the coefficient functions, since (4) yields the time average

$$\langle \mathcal{K}_{TD}(\mathcal{L}_n, t)\rangle_t = \langle -L_p\rangle_t + \langle \eta_1\rangle_t \mathcal{L}_n + \langle \eta_2\rangle_t \mathcal{L}_n^2 + \cdots \tag{12}$$

where the Ermakov–Lewis invariant is already quantized in equation (8). In (12) $\langle \eta_1\rangle_t$ is interpreted as the average angular velocity of the *linearized* tube motion. It obviously plays an important role for the identification of resonances. On the other hand, the average angular velocity of extended tubes (obtained by differentiating (12) with respect to $\mathcal{L}_n$) depends on the value of the Ermakov–Lewis invariant $\mathcal{L}_n$, which is the main nonlinear manifestation. The 'softening' or 'stiffening' behaviour of the local oscillator is typically determined by the quantity $\langle \eta_2\rangle_t$.

3. Resonance limitations

The order of truncation of the normal-form Hamiltonian depends on the existence of a highest index N of a periodic coefficient function $\eta_N(t)$. The coefficients are, as we shall see, subject to certain non-resonant conditions of the angular velocity (or winding number) of the linearized flow near the periodic centre. A closer look at the leading coefficient functions in (4) shows that they are expressed in terms of two types of functions intrinsic to the time-dependent normal-form theory. According to [4] and [11], the leading normal-form coefficient is given by

$$\eta_1(t) = \rho^{-2}(t). \tag{13}$$

where the real and positive function $\rho(t)$ is a periodic Milne solution, satisfying

$$\ddot{\rho}(t) + h_2(t)\rho(t) = \rho^{-3}(t). \tag{14}$$

For the sake of simplicity we have suppressed an additional parameter in equations (13) and (14) that can be eliminated by rescaling the Milne solution [11].

The second, complete normal-form coefficient was first derived in [4]:

$$\eta_2(t) = \tfrac{3}{8}h_4(t)\rho^4(t) + \tfrac{3}{2}h_3(t)\rho^3(t)(\mathrm{Im}\, a_{21}(t) - \mathrm{Im}\, a_{30}(t)) \tag{15}$$

where $a_{kl}(t)$ are solutions of the following type of linear equations:

$$\dot{a}_{kl}(t) + \mathrm{i}\eta_1(t)(k-l)a_{kl}(t) = 2\mathrm{i}f_{kl}(t) \qquad k+l = 3, 4, \ldots. \tag{16}$$

The driving functions $f_{kl}(t)$ on the right-hand side are always periodic and known from earlier transformation steps. Previously an incomplete approximation of the second normal-form coefficient was given in [6]:

$$\eta_2^1(t) = \tfrac{3}{8}h_4(t)\rho^4(t) \tag{17}$$

neglecting the leading (cubic) transformation functions $a_{21}(t)$ and $a_{30}(t)$.

From the basic coefficient equations (13) and (15) we can see that the existence of a periodic Milne solution is the true 'bottle neck' of the narrow-tube quantization. This sets the main resonance limitation, which we shall describe below. Secondary resonances show up in the following transformation coefficients $a_{kl}(t)$, as they cease to exist despite an existing Milne solution.

3.1. Main resonance

We shall first assume that the centre motion is stable, which is at the very essence of the elliptic islands. The linearized flow

$$\ddot{Q}(t) + h_2(t)Q(t) = 0 \tag{18}$$

is then stable with periodic or quasiperiodic solutions only. Since the Milne, or amplitude solution $\rho(t)$ can be viewed as the radial motion in the plane of two fundamental solutions $Q_1(t)$ and $Q_2(t)$ as $\rho(t) = \text{constant} \times \sqrt{Q_1^2(t) + Q_2^2(t)}$ (see e.g. [3, 12, 13]), we have with our assumption secured the existence of a finite function $\rho(t)$ (at least). That it can also be found periodic follows from Floquet theory as described subsequently (an alternative argument is given in [13]).

With our assumption equation (18) has, since it is real, two fundamental Floquet solutions, which can be written formally as $P(t)\mathrm{e}^{\mathrm{i}\lambda t}$ together with its complex conjugate. Here $P(t)$ is a complex periodic function with the underlying Floquet period T_F, defined by the periodicity of the function $h_2(t+T_F) = h_2(t)$, and $\pm\mathrm{i}\lambda T_F$ are the imaginary characteristic exponents. Hence, λ corresponds to our average angular velocity $\langle\eta_1\rangle_t$. As real fundamental solutions $Q_1(t)$ and $Q_2(t)$ one may take the real and imaginary parts, hence yielding the suitable T_F-periodic $\rho(t) = \text{constant} \times \sqrt{P(t)P^*(t)}$.

Failure of finding a periodic Milne solution hinges on the independence of the fundamental Floquet solutions. Solutions are degenerate if for example $\pm\lambda = 0 (\mathrm{mod}\, 2\pi/T_F)$, but also if $\pm\lambda = \pm\pi/T_F (\mathrm{mod}\, 2\pi/T_F)$, since then $\mathrm{e}^{-\mathrm{i}(\pi/T_F)t} = \mathrm{e}^{-2\mathrm{i}(\pi/T_F)t}\mathrm{e}^{\mathrm{i}(\pi/T_F)t}$, and both Floquet solutions again become of the same form. We conclude that main resonances occur when

$$\lambda = \langle\eta_1\rangle_t = \pi/T_F (\mathrm{mod}\, \pi/T_F) \tag{19}$$

where typically $T_F = T_p/2$ or T_p, depending on the symmetry of the centre motion.

3.2. Secondary resonance

Returning to equation (16) for the transformation coefficients entering the normal form, it is straightforward to solve the linear equation with the additional periodicity requirement of the centre motion $a_{kl}(0) = a_{kl}(T_p)$. We find:

$$a_{kl}(0) = \frac{2\mathrm{i}\int_0^{T_p} f_{kl}(t)\mathrm{e}^{\mathrm{i}(k-l)\int_0^t \eta_1(x)\,\mathrm{d}x}\,\mathrm{d}t}{\mathrm{e}^{\mathrm{i}(k-l)\int_0^{T_p}\eta_1(t)\,\mathrm{d}t} - 1}. \tag{20}$$

In particular, we see the breakdown of the formula whenever

$$\int_0^{T_p} \eta_1(t)\,\mathrm{d}t = \frac{2\pi j}{k-l} \tag{21}$$

for any integers j, k and $l \neq k$. Hence, the winding angle over one centre period cannot be an integral fraction of 2π, or multiples thereof. For the leading higher-order normal-form coefficient we need only worry about the case $k + l = 3$, i.e. the winding angles $2\pi/3, 4\pi/3, \ldots$ and the vanishing or complete ones, already excluded by the main resonance restriction.

4. Application to the forced Duffing oscillator

The explicit form of the unit mass Hamiltonian Duffing oscillator is given by

$$H(p_x, x, t) = \tfrac{1}{2}p_x^2 + \tfrac{1}{2}kx^2 + \tfrac{1}{4}sx^4 - rx\cos t \tag{22}$$

where k is the linear oscillator stiffness and s is the nonlinearity strength. By the canonical periodic-centre transformation, we obtain the basic 'centre' Hamiltonian (3) with (see e.g. [6])

$$-L_p(t) = -\tfrac{1}{2}\dot{x}_p^2 + \tfrac{1}{2}kx_p^2 + \tfrac{1}{4}sx_p^4 - rx_p\cos t \tag{23}$$

$$h_2(t) = k + 3sx_p^2 \tag{24}$$

$$h_3(t) = 3sx_p \tag{25}$$

$$h_4(t) = s. \tag{26}$$

In the numerical calculations we consider the dominating harmonic centres of period $T_p = T = 2\pi$, and a subharmonic centre with period $T_p = 3T = 6\pi$. We observe that the centre motion $x_p(t)$ for the Duffing oscillator enters quadratically in $h_2(t)$, which makes this coefficient $T_p/2$-periodic for symmetric responses. The period of the Milne solution $\rho(t)$ is then also $T_p/2$. On the other hand, $h_3(t)$ has the period T_p.

The higher-order transformation coefficients $a_{kl}(t)$ in (16) require explicit expressions for the functions $f_{kl}(t)$. They, in turn, have already been worked out in [4] for the leading orders. We have

$$f_{3-l,l}(t) = \frac{1}{3}h_3(t)\rho^3(t)\left(-\frac{\mathrm{i}}{2}\right)^3\binom{3}{l}(-1)^l \tag{27}$$

which together with (25) leads to the two equations:

$$\dot{a}_{30}(t) + 3\mathrm{i}\eta_1(t)a_{30}(t) = -\tfrac{1}{4}sx_p(t)\rho^3(t) \tag{28}$$

and

$$\dot{a}_{21}(t) + \mathrm{i}\eta_1(t)a_{21}(t) = \tfrac{3}{4}sx_p(t)\rho^3(t). \tag{29}$$

The expression for the coefficient $\eta_2(t)$ in (15) indicates a significant contribution through $a_{30}(t)$ and $a_{21}(t)$ from the cubic coefficient $h_3(t)$ of the centre Hamiltonian (3) that was previously neglected in the narrow-tube quantization [6]. One can expect in adiabatic or quasistationary situations that $a_{21}(t)$ will be the larger of the two transformation coefficients. In fact, in [4] the adiabatic expressions were derived with the results:

$$a_{30} = \frac{\mathrm{i}h_3}{36h_2^{5/4}} \tag{30}$$

$$a_{21} = -\frac{\mathrm{i}h_3}{4h_2^{5/4}}. \tag{31}$$

In such an approximation we see that these coefficients are imaginary.

4.1. T-periodic centres

We take a look at the perturbed harmonic oscillator ($s = 0.03$, $r = 0.5$) previously studied in [6]. For $k > 1$ the oscillator has a single stable harmonic response dominating the phase-space map, whilst for $k < 1$ two stable centres (referred to as of *large amplitude* and *small amplitude* in this paper) prevail. As is well known, the single centre for $k > 1$ continues smoothly to the large-amplitude centre for $k < 1$. The small-amplitude centre bifurcates

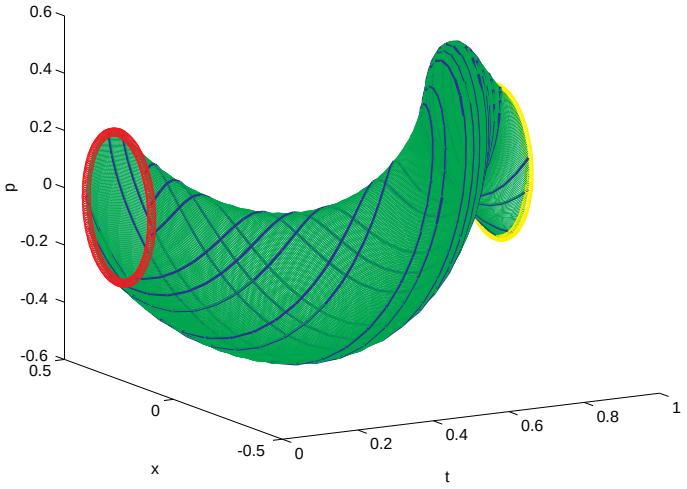

Figure 1. Illustration of adiabatic T-harmonic vortex tube. The weakly nonlinear Duffing system described in the text has a stiffness $k = 3$.

near resonance $k \approx 1$ together with a hyperbolic fix point (unstable response). Initially we would like to numerically analyse the situations in which the second coefficient $\eta_2(t)$ becomes small, as is the case for the single-amplitude (i.e. $k > 1$) and large-amplitude (for $k < 1$) centres.

4.1.1. Adiabatic behaviour. At large positive k the single centre, as for example the centre of the tube in figure 1, has a relatively small amplitude. This situation is ideal for the *adiabatic approximation* of the Milnes solution $\rho(t) \approx (k + 3sx_p(t))^{-1/4}$, obtained by neglecting the time derivative in (14) and inserting (24). The almost-constant behaviour of $\rho(t)$ carries through to the smooth behaviour of $a_{30}(t)$ and $a_{21}(t)$, which can also be obtained by a similar adiabatic approximations of equations (28) and (29). The vortex tube in figure 1 is consequently very much like the traditional ones drawn by hand, and we do not intend to analyse it further.

4.1.2. Non-adiabatic behaviour. As k decreases through zero, turning the oscillator to its double-well characteristics, the adiabatic behaviour gradually disappears, whilst the centre remains stable. Surprisingly the normal-form expansion in table 1 seems to converge rapidly, allowing larger values of the Ermakov–Lewis invariant and, hence, an accurate description of more quantum states supported by the elliptic centre. However, it turns out to be dangerous to neglect any of the terms in formula (15) for the coefficient $\eta_2(t)$. In [6] the authors noted that a crude approximation $\eta_2^1(t)$ (cf formula (17)) of the coefficient $\eta_2(t)$, obtained by a simplified averaging procedure, did not improve the lowest-order narrow-tube formula as it did in other situations. The corresponding non-adiabatic flux tube for $k = -2$, looking flat and simple-folded, is illustrated in figure 2; analysed in its transformation components in figure 3 and its normal-form components in figure 4.

In figure 3 the top left subplot shows the periodic centre motion $x_p(t)$ together with the corresponding periodic Milne solution (broken line), and the top right subplot shows the approximation $\eta_2^1(t)$ given by formula (17), which is just the contribution from the quartic

Table 1. $s = 0.03$, $r = 0.5$. Time averages of normal-form expansion coefficients for T-periodic centres.

k	x_0	$\langle\eta_0\rangle_t$	$\langle\eta_1\rangle_t$	$\langle\eta_2^1\rangle_t$	$\langle\eta_2\rangle_t$
Single centre					
3	0.249 844	−0.031 239	1.732 861	0.003 75	0.003 73
1.5	0.961 024	−0.122 410	1.241 404	0.007 32	0.005 69
Large-amplitude centre					
0.618^2	5.699 981	−3.421 941	1.156 081	0.046 19	−0.001 15
−1	10.015 221	−23.085 324	1.162 717	0.136 83	−0.000 71
−2	12.469 262	−47.791 944	1.165 039	0.253 62	−0.000 56
Small-amplitude centre					
0.6633	−2.200 821	0.208 674	0.975 139	0.106 17	11.312 34
0.618^2	−0.830 272	0.102 387	0.642 738	0.027 26	0.030 83
0.097	−0.558 188	0.069 482	0.333 228	0.101 32	6.972 14
−0.01	−0.497 901	0.062 052	0.034 157	9.643 03	10.299 30

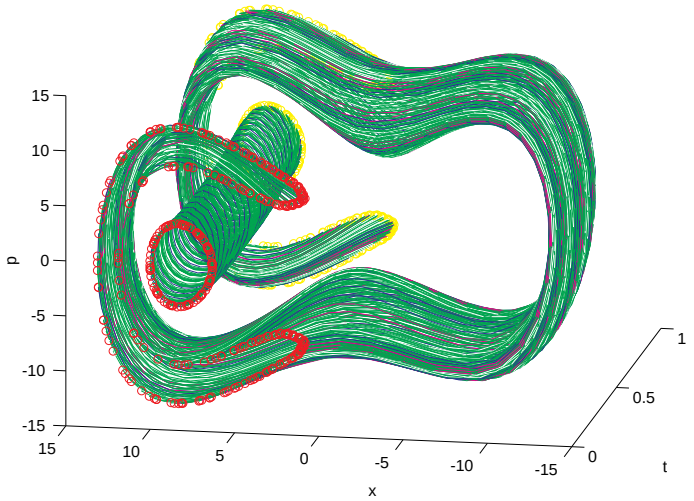

Figure 2. Illustration of two different T-harmonic vortex tubes for $k = -2$. The non-adiabatic tube discussed in the text winds both wells in the 'double-well' oscillator, partly surrounding an adiabatic tube localized in a single well.

part of the basic centre Hamiltonian to the normal form coefficient $\eta_2(t)$. The bottom subplots show the transformation coefficients $a_{30}(t)$ and $a_{21}(t)$ caused by the cubic terms of the basic centre Hamiltonian. They show a T-periodic behaviour with distinct spikes at times $t = 0$ and $T/2 \pmod T$.

The complete normal-form coefficients $\eta_1(t)$ and $\eta_2(t)$ are finally compared in figure 4. The first of these coefficients has prominent spikes at $t = 0$ and $T/2 \pmod T$ when it dominates the normal form. The second coefficient $\eta_2(t)$ looks smoother than the transformation coefficients $a_{30}(t)$ and $a_{21}(t)$ suggested in figure 3. Their spikes are suppressed by the simultaneous smallness of the factor $\rho^3(t)$ in formula (15). It is seen that $\eta_2(t)$ also differs from $\eta_2^1(t)$ of figure 3, explaining a much smaller averaged value.

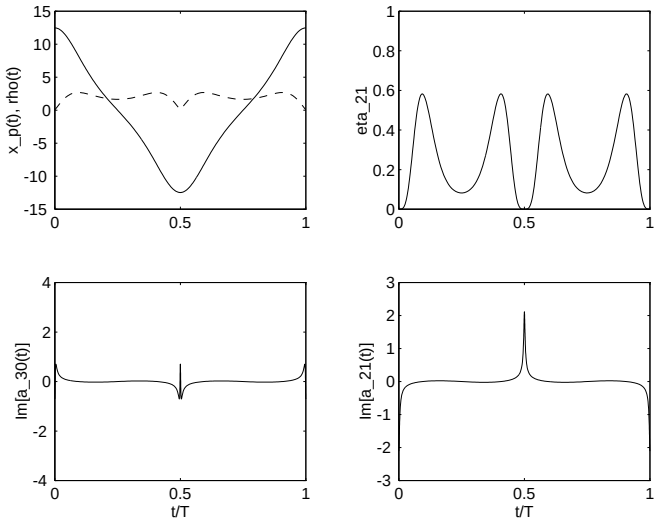

Figure 3. Analysis of transformation components for the non-adiabatic flux tube of figure 2 at $k = -2$.

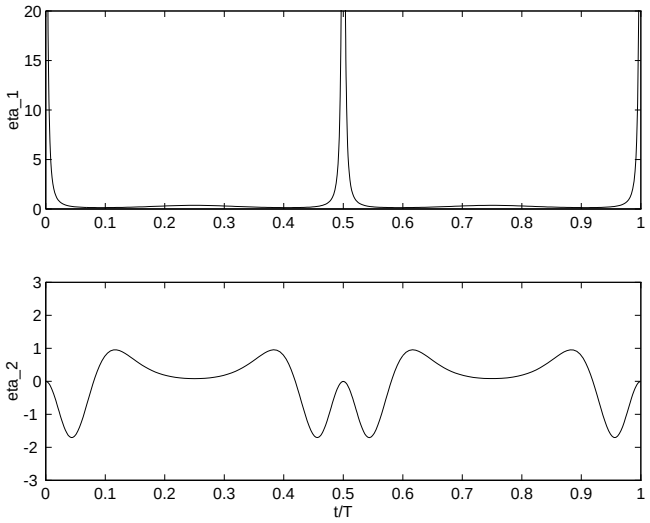

Figure 4. Time dependence of normal-form coefficients for the non-adiabatic flux tube of figure 2.

However, $\eta_2(t)$ is still relatively large compared with $\eta_1(t)$ at significant time intervals inside the period cycle.

Another important observation in figure 4 is that both normal-form coefficients have the period $T/2$, although we have only proved this behaviour for the first one $\eta_1(t)$. In formula (15) it is the product of the centre motion symmetry $x_p(t + T/2) = -x_p(t)$ and the same symmetry of the transformation coefficients that has this effect.

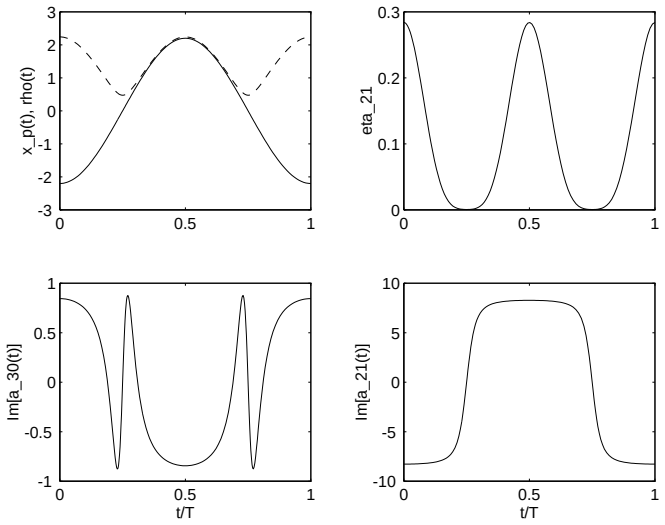

Figure 5. Analysis of small-amplitude centre components for k =0.6633.

4.1.3. Main resonances. We did not observe any resonance breakdown of the normal form coefficients for the large-amplitude/single-harmonic centre in the parameter region considered. This appears instead in the small-amplitude harmonic centre, which is stable in the limited approximate parameter range $-0.010 < k < 0.663$. In table 1 we see that the time-averaged coefficient $\langle \eta_2(t) \rangle_t$ for the small-amplitude centre becomes large compared with $\langle \eta_1(t) \rangle_t$ close to the stability limits, while being small in the middle of the stability interval. We conclude that at $k = 0.6633$ we are close to a main resonance, since $\langle \eta_1 \rangle_t \approx 1$ according to table 1. When studying the analysis of the basic quantities in figure 5 and its consequences on the time behaviour of the normal-form coefficients in figure 6, we observe a weakly singular behaviour of Milne's amplitude solution, becoming the finite absolute value of $x_p(t)$. The time behaviour of the coefficient $\eta_2(t)$ in figure 6 shows again a period of $T/2$. $|\eta_2(t)|$ becomes particularly large at times $t = 0, T/4, T/2, \ldots$, where it dominates the linear coefficient $\eta_1(t)$.

A different (not illustrated) singular behaviour of the Milne solution is encountered when analysing the other end (see $k = -0.01$ in table 1) of the stability interval. This is a main resonance with $\langle \eta_1 \rangle_t \approx 0$. Here the centre amplitude is very small, but still the Milne solution becomes very large (eventually infinite).

4.1.4. Secondary resonances. We turn to purely secondary resonances of the small-amplitude centre. At $k = 0.097$ we are close to a secondary $3T$-resonance, since $\langle \eta_1 \rangle_t \approx \frac{1}{3}$ in table 1. This resonance shows up, due to condition (21), as an unusually large transformation coefficient $a_{30}(t)$, which in turn is causing the large normal-form coefficient $\eta_2(t)$. We can confirm, in figures 7 and 8, that the Milne solution is regular and not responsible for the large $\eta_2(t)$. Although the Milne solution is almost constant, the situation is not adiabatic. We also recall that $a_{21}(t)$ should be the largest of the transformation coefficients in adiabatic situations.

4.1.5. Quasienergies. To close this section, we compare, in table 2, the first- and second-order quasienergies given by formula (11) with the semiclassical EBK results already

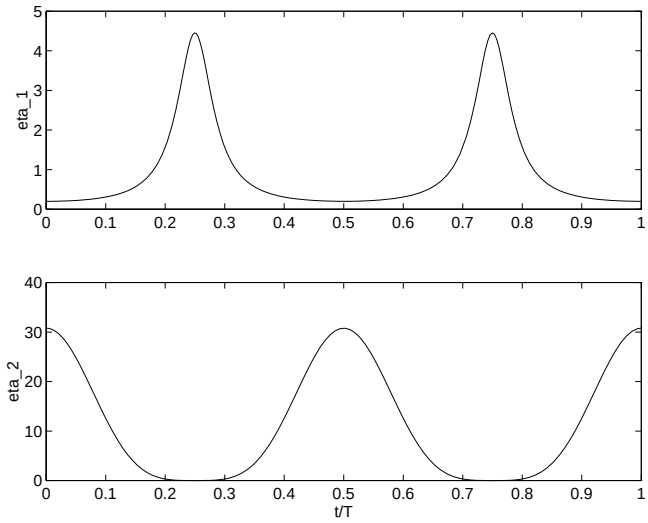

Figure 6. Time dependence of normal-form coefficients for the motion near the small-amplitude centre at $k = 0.6633$.

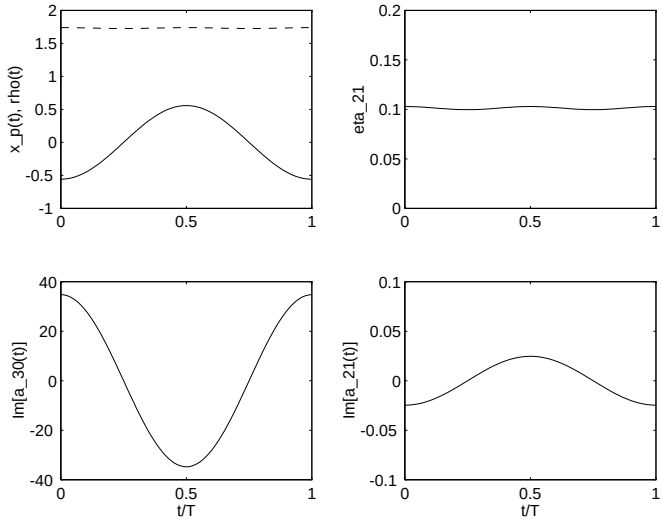

Figure 7. Analysis of the small-amplitude centre components near a subharmonic $3T$-resonance at $k = 0.097$.

published in [6]. Numerically, we use the value $\overline{h} = 1$ in our calculations. The second-order narrow-tube results are consistently better than the first-order ones for the leading 'principal' quasienergies. This may be due to the non-resonant parameter values chosen for the comparison. The experience in [6] with the large-amplitude elliptic centre was that the crude higher-order approximation would shift the first-order quasienergies in the wrong direction. This is confirmed in the corresponding entries of table 1.

We finally note that both EBK and narrow-tube quantizations have an absolute energy scale to the principal part of the quasienergies, in contrast to the quantal numerical methods.

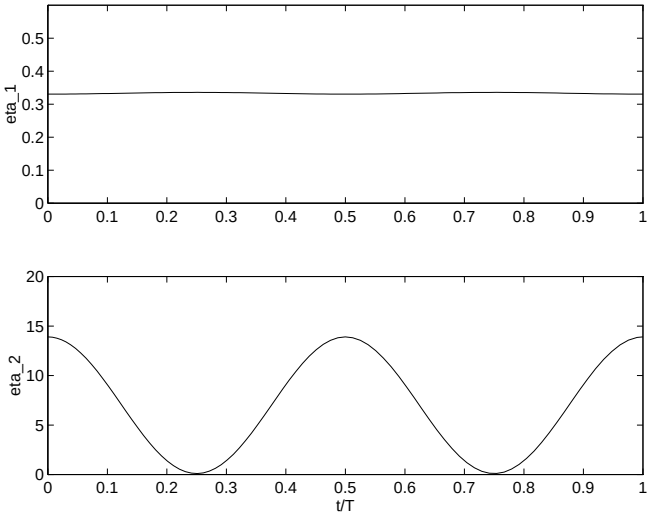

Figure 8. Time dependence of normal-form coefficients for the motion near the small-amplitude centre near a subharmonic $3T$-resonance at $k = 0.097$.

Table 2. Quasienergies located at the large-amplitude and small-amplitude elliptic centres. Parameters are found in table 1 and [3].

x_0	n	ϵ_1^{NT}	ϵ_2^{NT}	ϵ^{SC}
5.699 98	0	−2.8439	−2.8442	−2.8445
	1	−1.6878	−1.6904	−1.6907
	2	−0.5317	−0.5389	−0.5391
	3	0.6243	0.6103	0.6096
−0.830 27	0	0.4238	0.4315	0.4312
	1	1.0665	1.1359	1.1309
	2	1.7092	1.9019	1.8834
	3	2.3520	2.7296	2.6930

4.2. 3T-periodic centre

We would also like to establish the time-dependent normal form for quantizing motion *inside* subharmonic resonance islands. The first investigation of the quasienergy spectrum corresponding to subharmonic motion seems to be that of Holthaus and Flatte [14].

Here we are interested in a particular subharmonic centre motion for the Duffing oscillator given by (see [15]):

$$x_p(t) = 2\left(\frac{r}{2}\right)^{1/3}\cos(t/3) \tag{32}$$

where the quenching of higher harmonics is achieved by a specific relation between the excitation amplitude and the linear spring constant:

$$r = 2(\tfrac{1}{27} - k/3)^{3/2} > 0. \tag{33}$$

The simple form of the subharmonic centre motion (32) makes it suitable for the analytic transformation of the Hamiltonian. The resulting analytic expression for $h_2(t)$ also makes the stability analysis of the centre motion rigorously understood from the Mathieu equation [16].

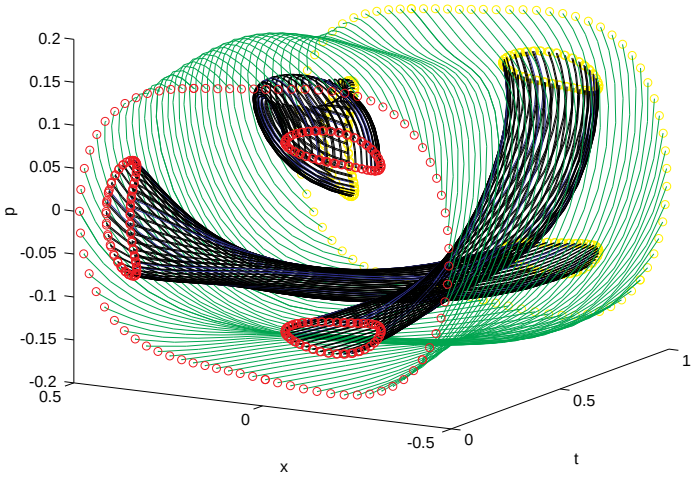

Figure 9. Illustration of T-harmonic and $3T$-subharmonic vortex tubes.

In the relevant parameter region the oscillator develops from the single-well character ($0 < k < \frac{1}{9}$) to the double-well character ($k < 0$). In order to sustain the centre motion (32) the excitation is adjusted to fulfil the quenching condition above. The solution exists for all $k < 0$ and its amplitude tends to infinity in the limit $k \to -\infty$. However, it passes through alternately stable and unstable intervals, the latter rapidly becoming larger and larger [16]. The largest stability interval being $-0.166\,66 < k < 0.111\,111$.

For $k = 0$ and $s = 1$ we then have a particular driven quartic Ueda oscillator, which shows quite dense phase-space structures corresponding to various subharmonic motions, as reported by Mirbach and Korsch [17] and Korsch *et al* [18]. From such a view of phase space, one expects that some quasienergies are dominated by the subharmonic motion, and the $3T$-islands clearly dominate a considerable region of phase space, not too far from the origin.

In figure 9 we have illustrated the disconnected subharmonic vortex tubes in the period-T interval, surrounded by a harmonic tube of larger amplitude. With a sufficiently small value of $\overline{h}$ (in the calculations we have $\overline{h} = 0.0005$) there will exist some quasienergy states localized to such vortex tubes. Mirbach and Korsch [17] and Korsch *et al* [18] have performed semiclassical EBK calculations of quasienergies and compared the results with exact quantal ones. Their studies also comprise the extended states, influenced by tunnelling between the subharmonic tubes through the (chaotic) hyperbolic ridges.

To establish the narrow-tube quantization formula (11) we first note that the time-averaged quantities $\langle \eta_0(t) \rangle_t$, etc are all calculated over the centre period $3T$ and the Brillouin-zone multiples are in units of $\overline{h}/3$. In table 3 we study the averaged normal-form coefficients inside the main stability interval mentioned earlier. The second-order coefficient is generally of a much larger magnitude in this case, allowing reliable second-order applications only to small values of the Ermakov–Lewis invariant. Close to the main stability loss it increases even more. We notice that $T_F = T_p/2 = 3\pi$, so that the main resonances (see equation (19)) occur for $\langle \eta_1 \rangle_t = \frac{1}{3} (\mathrm{mod}\ \frac{1}{3})$.

In table 4 we study the first- and second-order narrow-tube approximations of the leading principal quasienergies on the absolute scale given by classical mechanics. The quantal

Table 3. $s = 1$, $r = 2(\frac{1}{27} - k/3)^{3/2}$. Centre fix point and averaged normal-form coefficients.

k	x_0	$\langle\eta_0\rangle_t$	$\langle\eta_1\rangle_t$	$\langle\eta_2^1\rangle_t$	$\langle\eta_2\rangle_t$
−0.16	0.601 2333	−0.012 2502	0.621 897 38	17.9858	−24.7823
0	0.384 9002	−0.002 0576	0.405 525 41	10.3894	−2.8687
0.10	0.121 7161	−0.000 0206	0.335 927 57	188.9330	−3.6834

Table 4. Principal quasienergies for subharmonic elliptic centre at $k = 0$. Exact results are transformed to our energy scale from [9].

x_0	n	ϵ_1^{NT}	ϵ_2^{NT}	ϵ^{Exact}
0.384 9002	0	−0.001 956 23	−0.001 956 41	−0.001 956 49
	1	−0.001 753 47	−0.001 755 08	−0.001 755 22
	2	−0.001 550 71	−0.001 555 19	−0.001 555 50
	3	−0.001 347 94	−0.001 356 73	−0.001 357 46
	4	−0.001 145 18	−0.001 159 70	−0.001 161 23
	5	−0.000 942 42	−0.000 964 11	−0.000 967 03

results are carefully traced back from [17] to this scale by adding or subtracting multiples of $\bar{h}/3$. The improvement provided by the second-order contribution is easily destroyed if the crude approximation $\langle\eta_2^1\rangle_t$ is used instead of $\langle\eta_2\rangle_t$ (see table 3).

5. Concluding remarks

In this study we show that the narrow-tube quantization is reliable for calculating quasienergies associated with regular phase-space motion near stable periodic orbits. Comparisons with EBK and full quantal calculations are in very good agreement, with significant contributions from the higher-order normal-form terms. We note that these quasienergies and the corresponding localized Floquet states seem to be related to the 'Trojan wavepackets' of Kalinsky and Eberly [19] and the 'non-spreading wavepackets' by Buchleitner and Delande [20].

With the narrow-tube quantization we gain a pictorial understanding of various sequences of quasienergies corresponding to elliptic islands of phase space. The position on the quasienergy scale is governed by the zeroth-order contribution $\langle\eta_0(t)\rangle_t$, which is the negative Lagrangian action of the centre motion. This corresponds to the depths of various ordinary energy wells. Then the sequence of states 'inside each well' is a fingerprint of the structure of the well. The well shape, for example, is related to the 'oscillation period' which in turn corresponds to the angular velocity of the oscillatory motion. In a quasienergy-versus-quantum number plot, the contributions from elliptic islands will thus appear as a patchwork of sequences of states with characteristic positions and slopes.

We observed that the second-order time-dependent normal form possessed a stronger symmetry than the basic centre Hamiltonian suggested. Specifically, *all* coefficients of the normal form have a period of $T/2$, which is not the case in the original centre Hamiltonian. Consequently, the angular velocities on the considered T-periodic vortex tubes rather show a $T/2$-periodic behaviour. This behaviour is a consequence of the symmetry $x_p(t + T/2) = -x_p(t)$ of the centre motion. A similar result can be shown for the $3T$-periodic vortex tube in our study.

References

[1] Thylwe K-E and Dammert Ö 1994 *J. Phys. A: Math. Gen.* **27** 4011
[2] Vattay G, Wirzba A and Rosenqvist P E 1994 *Phys. Rev. Lett.* **73** 2304
[3] Fröman N and Fröman P O 1996 *Phase-integral Method: Allowing Nearlying Transition Points (Springer Tracts in Natural Philosophy 40)* (New York: Springer) ch 2, pp 26–34
[4] Thylwe K-E and Dankowicz H 1996 *J. Phys. A: Math. Gen.* **29** 3707
[5] Thylwe K-E and Dankowicz H 1997 *J. Phys. A: Math. Gen.* **30** 111
[6] Thylwe K-E and Bensch F 1994 *J. Phys. A: Math. Gen.* **27** 5673
[7] Breuer H P and Holthaus M 1991 *Ann. Phys., NY* **211** 249
[8] Bensch F, Korsch H J, Mirbach B and Ben-Tal N 1993 *J. Phys. A: Math. Gen.* **25** 6761
[9] Howland J S 1992 *J. Phys. A: Math. Gen.* **25** 5177
[10] Hone D W, Ketzmerick R and Kohn W 1997 *Phys. Rev.* A **56** 4045
[11] Thylwe K-E and Bensch F 1994 *J. Phys. A: Math. Gen.* **27** 7475
[12] Lewis H R 1968 *J. Math. Phys.* **9** 1976
[13] Nuñez J A, Bensch F and Korsch H J 1994 *J. Phys. A: Math. Gen.* **24** 2069
[14] Holthaus M and Flatte S 1994 *Phys. Lett.* A **187** 151
[15] Thylwe K-E 1993 *J. Sound Vibration* **161** 203
[16] Gravador E, Thylwe K-E and Hökback A 1995 *J. Sound Vib.* **169** 214
[17] Mirbach B and Korsch H J 1996 *J. Phys. A: Math. Gen.* **27** 7475
[18] Korsch H J, Mirbach B and Schellhaaß B 1997 *J. Phys. A: Math. Gen.* **30** 1659
[19] Kalinsky M and Eberly J H 1996 *Phys. Rev.* A **53** 1715
[20] Buchleitner A and Delande D 1995 *Phys. Rev. Lett.* **75** 1487